Available online at www.sciencedirect.com
ScienceDirect
Trans. Nonferrous Met. Soc. China 28(2018) 1618−1625
Transactions of Nonferrous Metals Society of China
www.tnmsc.cn

Enhanced dehydrogenation kinetic properties and hydrogen storage reversibility of $LiBH_4$ confined in activated charcoal

He ZHOU[1], Hai-zhen LIU[2], Shi-chao GAO[1], Xin-hua WANG[1]

1. State Key Laboratory of Silicon Materials, School of Materials Science and Engineering, Zhejiang University, Hangzhou 310027, China;
2. State Key Laboratory of Advanced Transmission Technology, Global Energy Interconnection Research Institute, State Grid Corporation of China, Beijing 102209, China

Received 29 March 2017; accepted 19 June 2017

Abstract: $LiBH_4$ was confined into activated charcoal (AC) by melt infiltration method (MI), and its effects on the hydrogen sorption properties were investigated. The N_2 adsorption results reveal that melt infiltration method can effectively incorporated $LiBH_4$ into AC. It can maintain the structural integrity of the scaffold and ensure the confinement effect. The nano-confined $LiBH_4$/AC starts to release hydrogen at around 190 °C, which is 160 °C lower than that of pure $LiBH_4$, and reaches a hydrogen desorption capacity of 13.6% at 400 °C. When rehydrogenated under the condition of 6 MPa H_2 and 350 °C, it has a reversible hydrogen storage capacity of 6%, while pure $LiBH_4$ shows almost no reversible hydrogen storage capacity under the same condition. Mass spectrometry analysis (MS) results suggest that no diborane or other impurity gases are released in the decomposition process. The apparent activation energy of dehydrogenation of $LiBH_4$ after confinement into AC decreases from 156.0 to 121.1 kJ/mol, which leads to the eminent enhancement of dehydrogenation kinetics of $LiBH_4$.

Key words: hydrogen storage materials; hydrogen storage properties; lithium borohydride; activated charcoal; melt infiltration

1 Introduction

As the world is facing an increasing energy demand and is in an urgent need of a cleaner and more environmentally friendly energy storage technology, hydrogen energy comes into people's sight [1,2]. Hydrogen is considered to be an important potential energy carrier system, which can facilitate efficient utilization of unevenly distributed renewable energy [3−5]. Right now, safe and efficient hydrogen storage has been generally recognized as the key technical challenge in the utilization of hydrogen energy. A new class of lightweight materials for hydrogen storage are complex hydride and they have attracted much attention since the first publication on the reversible Ti catalyzed $NaAlH_4$ and Na_2LiAlH_6 by BOGDANOVIĆ and SCHWICKARDI [6]. Currently, $LiBH_4$ is one of the most attractive candidates for on-board hydrogen storage because of its high gravimetric hydrogen density (18.5%) and volumetric density (121 kg/m^3) [7,8]. However, release and uptake of hydrogen only take place under very extreme conditions (400 °C for release, and more than 400 °C and more than 10 MPa H_2 for uptake) due to its high thermodynamic stability (ΔH=75 kJ/mol) and kinetic restrictions [9,10].

Several strategies have been developed to tackle the thermodynamic and/or kinetic problems imposed by the strong and directional B—H bonds in $LiBH_4$ [9,11]. The strategies include reactant destabilization [12−16], nano-confinement [17−20], catalyst doping [21−24], and cation/anion substitution [25−27]. These strategies have all been proved to be feasible to improve the dehydrogenation of $LiBH_4$. Among them, nano-confinement can be very effective in improving the kinetic and thermodynamic properties of $LiBH_4$ [28]. The practical application of mesoporous carbon and silica has been proved functionally by several reports [17,29]. The confinement of metal hydrides in a

Foundation item: Projects (51471149, 51771171) supported by the National Natural Science Foundation of China; Project (2015C31029) supported by Public Project of Zhejiang Province, China
Corresponding author: Xin-hua WANG; Tel/Fax: +86-571-87952716; E-mail: xinhwang@zju.edu.cn
DOI: 10.1016/S1003-6326(18)64804-6

mesoporous scaffold creates nanoparticles, which limits the particle size of the hydride to the pore size of the scaffold material [30]. The particle size of the sample prepared by this way is considerably smaller than the one obtained by other methods like the mechanically milling.

Nanoconfinement efforts were initially put forward by GUTOWSKA and co-workers [31] for the study of hydrogen release from ammonia borane (NH_3BH_3) incorporated into mesoporous silica (SBA-15). They reported that the hydrogen release property is greatly improved compared with bulk samples. In addition, they suggested that the mechanism of the reaction is also modified. VAJO and co-workers [32] extended this nanoengineering method to the preparation of nanosized $LiBH_4$ samples. They succeeded in incorporating the hydride into mesoporous carbon aerogels, which demonstrated great improvement in H-exchange properties of $LiBH_4$, by using a melt infiltration method. Some researchers have focused on combining two different strategies to improve the properties. NIELSEN and co-workers [33,34] prepared a nanoconfined $2LiBH_4$−MgH_2 by melt infiltration method using carbon aerogel scaffold materials. The nano-confined $2LiBH_4$−MgH_2 samples show property advantages over their bulk counterpart, but the obtained kinetics improvement is much less distinguished. These studies have illustrated that create nanosized hydride is a promising route to improve hydrogen storage properties of $LiBH_4$ or any other complex hydride.

In this work, the recent efforts to improve the dehydrogenation and rehydrogenation properties of the nanoconfined $LiBH_4$ in porous activated charcoal (AC) prepared by melt infiltration (MI) were reported. Activated charcoal was used as a scaffold because it is relatively easy to acquire. Nanoconfined samples with a loading of around 35% $LiBH_4$ (which is calculated according to the pore volume of the scaffold) was prepared using MI method. The results show that confined $LiBH_4$ has improved dehydrogenation and rehydrogenation properties.

2 Experimental

$LiBH_4$ (95% purity) was purchased from Acros Organics and used without further purification. Activated charcoal (AC, 99% purity) was also purchased from Acros Organics and was purified under 500 °C and vacuum in a reactor for 5 h to remove moisture and other possible impurities. The $LiBH_4$/AC nanocomposite by MI (hereafter denoted as $LiBH_4$/AC-MI) was prepared following a two-step procedure. First, the $LiBH_4$ and AC scaffold were mixed using planetary mill at 100 r/min for 5 min. The mixture was then delivered into a reactor and calcined at 290 °C under 5 MPa H_2 pressure for 1 h. We also prepared a sample using hand milling for comparison (hereafter denoted as $LiBH_4$/AC-HM). This sample has the same $LiBH_4$/AC ratio, but was milled by hand in a mortar for 10 min in order to mix the sample homogeneously. All sample operations were performed in Ar atmosphere.

Dehydriding/rehydriding measurements were carried out on a homemade Sieverts-type apparatus. About 200 mg of sample was loaded into a stainless steel reactor, which was connected to a thermocouple and a pressure sensor to monitor the temperature and pressure inside the reactor. For the non-isothermal desorption measurements, i.e., the temperature programmed desorption (TPD) measurements, the samples were heated gradually from room temperature to 500 °C at a heating rate of 2 °C/min. For the isothermal desorption measurements, the samples were heated quickly to 350 °C under a back pressure of 5 MPa H_2 to prevent the decomposition of the samples. First, the tank connected to the reactor was evacuated. Then, the valve between the tank and the vacuum was turned off to maintain vacuum status in the tank. After that the valve between the tank and the reactor was opened to achieve a near vacuum state in the whole system to start the isothermal measurements. Hydrogen capacity was estimated by the ideal gas equation using the temperature and pressure previously obtained. The rehydriding process was carried out under the conditions of 350 °C and 6 MPa H_2. The reactor was filled with H_2 and then heated to 350 °C rapidly and kept at that temperature for 5 h.

The AC scaffold was characterized by gas absorption and desorption using an Autosorb-1-C surface area and pore size analyzer from Quantachrome. Differential scanning calorimetry (DSC) and thermogravimetric analysis (TG) were conducted using a differential scanning calorimeter (Netzsch STA449F3) equipped with a mass spectrometer (MS, Netzsch QMS−403C) to detect the hydrogen desorption synchronously. X-ray diffraction (XRD) analysis was performed on a PANalytical X-ray diffractometer (X'Pert Pro, Cu K_α, 40 kV, 40 mA), where the samples were sealed into a specially designed sample holder to avoid oxidation. Field emission scanning electronic microscopes (SEM, Hitachi S−4800) were applied to analyzing the morphology of the samples, while the energy dispersive spectroscopy (EDS) detector was used to study the elemental distributions.

3 Results and discussion

3.1 BET characterization and micropore analysis

The results of N_2 adsorption measurements of AC, $LiBH_4$/AC-MI and $LiBH_4$/AC-HM are shown in Fig. 1. The results of the BET and micropore analysis are

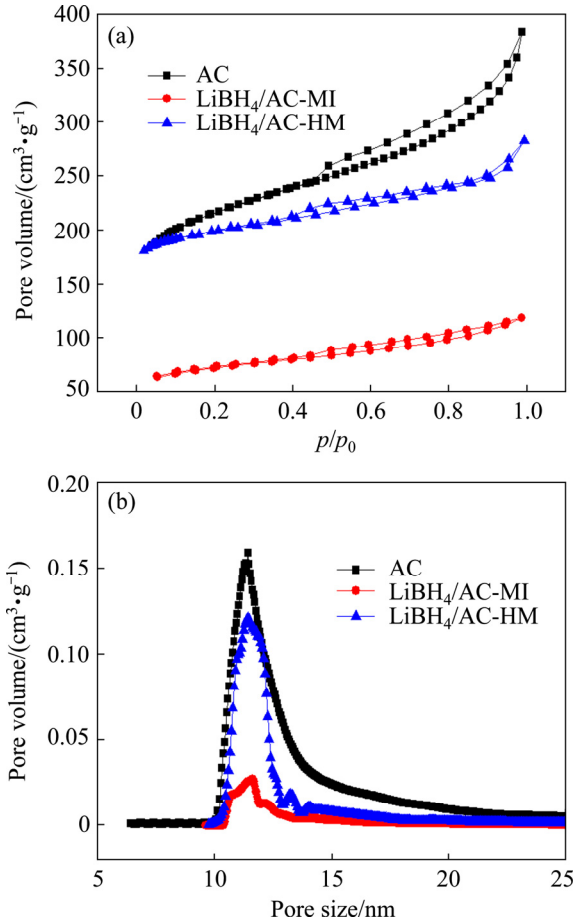

Fig. 1 BET measurements of AC scaffolds, $LiBH_4$/AC-MI and $LiBH_4$/AC-HM: (a) N_2 adsorption curves; (b) Pore size distribution

Table 1 Pore volume and specific surface area of AC scaffolds, $LiBH_4$/AC-MI and $LiBH_4$/AC-HM

Sample	Pore volume/ ($cm^3 \cdot g^{-1}$)	Specific surface area/($m^2 \cdot g^{-1}$)
AC	0.5836	2.921×10^2
$LiBH_4$/AC-MI	0.0886	6.54×10^1
$LiBH_4$/AC-HM	0.4595	2.212×10^2

summarized in Table 1, from which it can be seen that the specific surface area (SSA) of $LiBH_4$/AC-MI remarkably decreases after $LiBH_4$ was incorporated into the carbon scaffold, while it doesn't change much for $LiBH_4$/AC-HM. These results suggest that after the melt infiltration process, most of the porous structures are filled (or at least blocked) by $LiBH_4$. We also heated the AC scaffold with the same procedure as the MI process, which shows that the scaffold doesn't go through any structural transformation during the heating procedure. The decrease in the scaffold could only be the result caused by the incorporation of $LiBH_4$. According to Table 1, the pore volume difference between pure AC scaffold and $LiBH_4$/AC-MI sample is calculated to be 0.4950 cm^3/g. Combining this result with the density of $LiBH_4$, about 95% of the $LiBH_4$ sample is confined into the structure of carbon scaffold. The remaining 5% exists between the particles or on the surface of carbon scaffold. On the other hand, $LiBH_4$/AC-HM doesn't show much decrease in the surface area and the pore volume, which means that the hand mill sample remains the same porous structure as the original scaffold. The hand mill procedure only results in a physical mixture of $LiBH_4$ and the AC scaffold.

3.2 Dehydrogenation process

Figure 2 shows the TPD analysis profiles of $LiBH_4$/AC-MI. The results of $LiBH_4$/AC-HM and $LiBH_4$ are also shown for comparison. The samples are heated to 500 °C from room temperature at a heating rate of 2 °C/min. The dehydrogenation capacity is calculated based on the mass of $LiBH_4$, which means that the mass of the scaffolds is not taken into account when calculating the mass loss.

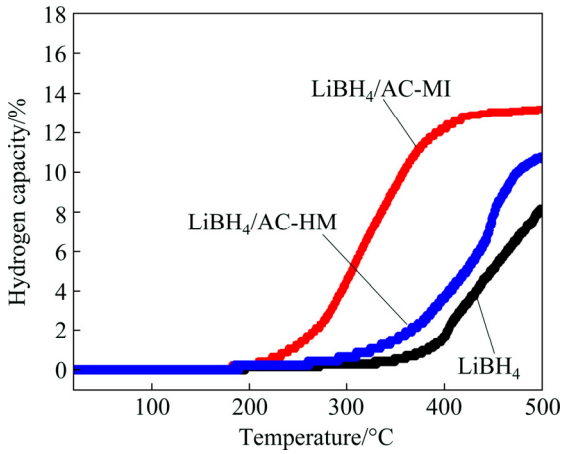

Fig. 2 TPD analysis profiles of $LiBH_4$/AC-MI, $LiBH_4$/AC-HM and $LiBH_4$

It can be clearly seen that the $LiBH_4$/AC-MI experiences a different dehydrogenation process. It starts to decompose at around 190 °C and finishes the decomposition process at around 400 °C. The dehydrogenation capacity reaches 13.6%. The bulk $LiBH_4$ starts to decompose at around 350 °C, and its decomposition is still not finished upon heating to 500 °C. $LiBH_4$/AC-HM sample also shows a decrease in the decomposition temperature. It starts to decompose at around 300 °C. After heating to 500 °C, it almost finishes the decomposition with a hydrogen capacity of 10.8%. We believe that AC scaffold may also have a catalytic effect on the dehydrogenation of $LiBH_4$, as the dehydrogenation temperature of the hand-milled sample is much lower than that of the pristine $LiBH_4$. So, it can be concluded that the melt infiltration process is successful, it provides a great enhancement on the

dehydrogenation of $LiBH_4$, leading to a 160 °C decrease in the onset dehydrogenation temperature. The enhancement might be a combined effect of nano-confinement and the catalytic effect of AC scaffold.

Figure 3 shows the synchronous DSC−TG−MS analysis results of $LiBH_4$/AC-MI. The heating rate is 8 °C/min. It is clear that the sample undergoes a phase transformation from orthorhombic to hexagonal structure at 116.0 °C and a melting process at 278.5 °C. The peak for the melting is much weaker than that of the pure $LiBH_4$, which indicates that $LiBH_4$ is in a polymorphic status and needs less energy to melt. After the melting, there is a tiny peak at 308 °C and a major hydrogen release step at 355.7 °C. Then, the final small peak at 461 °C might be caused by the decomposition of LiH.

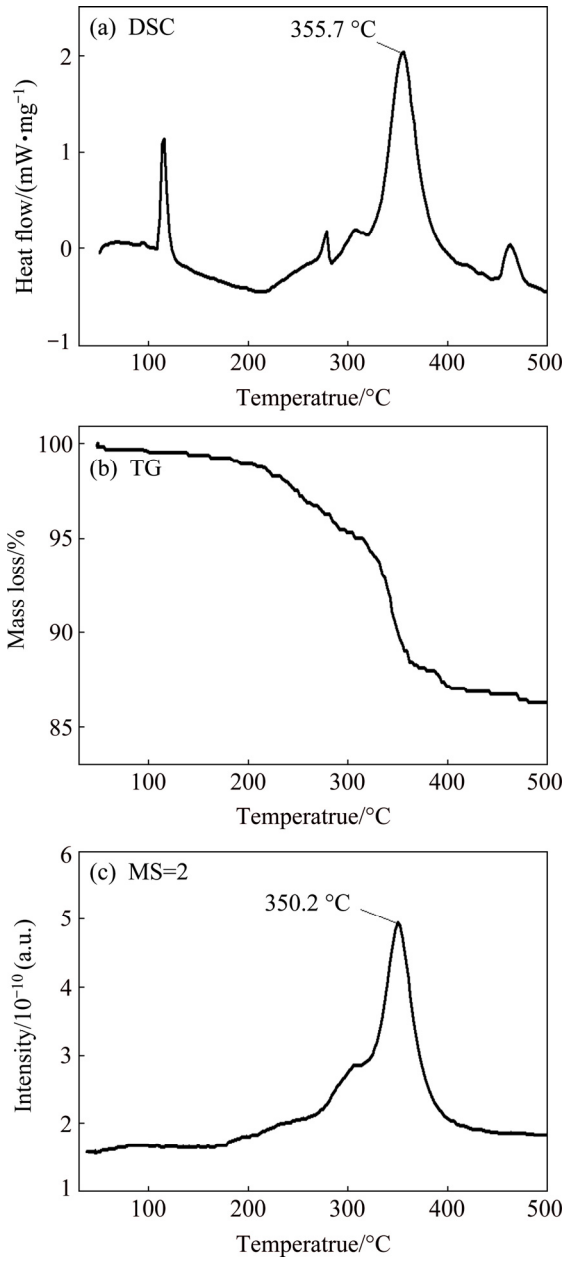

Fig. 3 Synchronous DSC−TG−MS analysis of $LiBH_4$/AC-MI

From the TG analysis, we can see that the sample starts to lose mass at around 185 °C, and finally reaches a mass loss of 13.6%. This is in accordance with the TPD results. According to the MS results, a hydrogen signal could be detected at around 185 °C, and the peak temperature for the hydrogen release is 350.2 °C. We could also see that the melting process is accompanied by a slight release of hydrogen.

To further understand the dehydrogenation mechanism of $LiBH_4$/AC-MI, we conducted XRD analysis on several stages during the dehydrogenation, and the results are shown in Fig. 4. According to the BET analysis results in Fig. 1, about 5% of the $LiBH_4$ is not confined into the AC scaffold. As nano-sized $LiBH_4$ does not show any diffraction peaks in XRD analysis, the peaks in Fig. 4 are probably induced by the remaining 5% of $LiBH_4$. It can be seen that no new crystalline phases are detected, the diffraction peaks of $LiBH_4$ are relatively weak, which indicates that $LiBH_4$ has lost part of its crystallinity. After heating the sample to 200 °C, the diffraction peaks of lithium hydride appear, this means that part of the sample starts to decompose. This confirms the onset dehydrogenation temperature obtained from previous analysis. After the sample is heated to 330 °C, the diffraction peak of lithium hydride

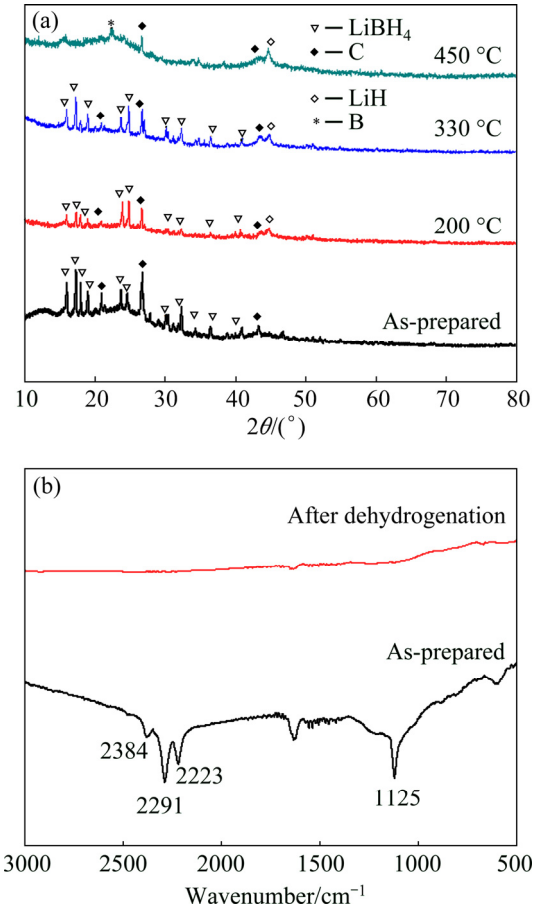

Fig. 4 XRD (a) and FTIR (b) patterns of $LiBH_4$/AC-MI heated to different temperatures

becomes more obvious in the sample. But the diffractions of carbon scaffolds and $LiBH_4$ are still visible. This indicates that the sample continues to decompose at this temperature, which is also the result we get from TPD and DSC analyses. After heating the sample to 450 °C, the diffraction peaks of carbon scaffolds are still visible, but those of $LiBH_4$ disappear completely, and the peaks of lithium hydride become more obvious. We can also find a diffraction peak located at 23°. This peak is probably caused by some kind of boron related phase, which is formed after $LiBH_4$ sample completely dehydrides. In this stage, $LiBH_4$ has completely decomposed into lithium hydride and hydrogen gas.

In order to further understand the decomposition mechanism of $LiBH_4$/AC-MI sample, FTIR is applied to analyzing the decomposition reaction. The FTIR results of the $LiBH_4$/AC-MI sample before and after dehydrogenation are shown in Fig. 4. It can be seen that the vibrational peaks of B—H stretching (2395, 2298 and 2234 cm^{-1}) and the bending (1125 cm^{-1}) are all shown in the as-prepared sample. This indicates that $LiBH_4$ presents in the as-prepared sample. When the sample is heated to 450 °C, the stretching and bending vibrational peaks all disappear, indicating the decomposition of $LiBH_4$ at this point. This confirms that the main hydrogen emission reaction occurs at ~300 °C.

3.3 Dehydriding kinetics

The dehydriding kinetics of $LiBH_4$/AC-MI is further studied by estimation of the kinetic barrier using the Kissinger method. The apparent activation energy (E_a) for the dehydriding reaction is determined by the following equation:

$$\ln\frac{c}{T_p^2}=-\frac{E_a}{RT_p}+A \quad (1)$$

where c is the heating rate in thermal analysis, T_p is the absolute temperature for the maximum reaction rate, R is the universal gas constant and A is also constant. In our study, the T_p data are extracted from the DSC measurements at various heating rates (c=5, 8, 12 and 16 °C/min), as demonstrated in Fig. 5(a). The apparent activation energy of the sample is estimated to be 121.1 kJ/mol (Fig. 5(b)), which is considerably lower than that of pure $LiBH_4$ (156 kJ/mol). The reduction in the apparent activation energy causes the improvement of dehydriding kinetic.

To further study the dehydrogenation kinetics of $LiBH_4$/AC-MI, we conducted isothermal dehydriding measurements. The results are shown in Fig. 6, from which it can be seen that melt infiltration process greatly improves the dehydrogenation kinetic of $LiBH_4$. For example, it only took 33 min to release about 9% of hydrogen. During the same period of time, $LiBH_4$/AC-HM only releases about 1% hydrogen, while pure $LiBH_4$ had barely started to decompose. $LiBH_4$/AC-MI can fully decompose within 1 h, and release approximately 10% hydrogen. This hydrogen capacity is lower than its theoretical one, which is 13.8%. We think that part of hydrogen was lost during the evacuating step. This step lasted around 20 s, during which the hydrogen loss could not be measured. Another reason is that the sample was not fully decomposed under this circumstance, resulting in the hydrogen capacity lost.

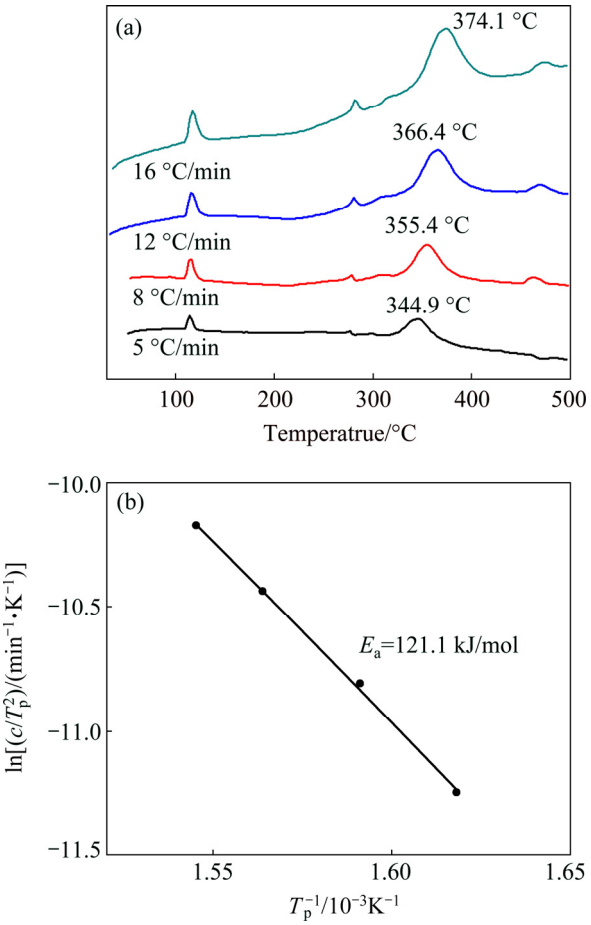

Fig. 5 DSC curves of $LiBH_4$/AC-MI under various heating rates (a) and apparent activation energy results determined by Kissinger method (b)

3.4 Rehydrogenation properties

In order to study the cyclic property, the samples are rehydrided for a second dehydrogenation cycles. First, the dehydrided samples are heated to 350 °C in vacuum. After a constant temperature of 350 °C is attained, 6 MPa hydrogen gas is pumped into the reaction chamber which starts the rehydriding process. The sample is held under the same environment for 5 h until the end of the dehydriding process. The first few cycles of the dehydrogenation curves are shown in Fig. 7. It can

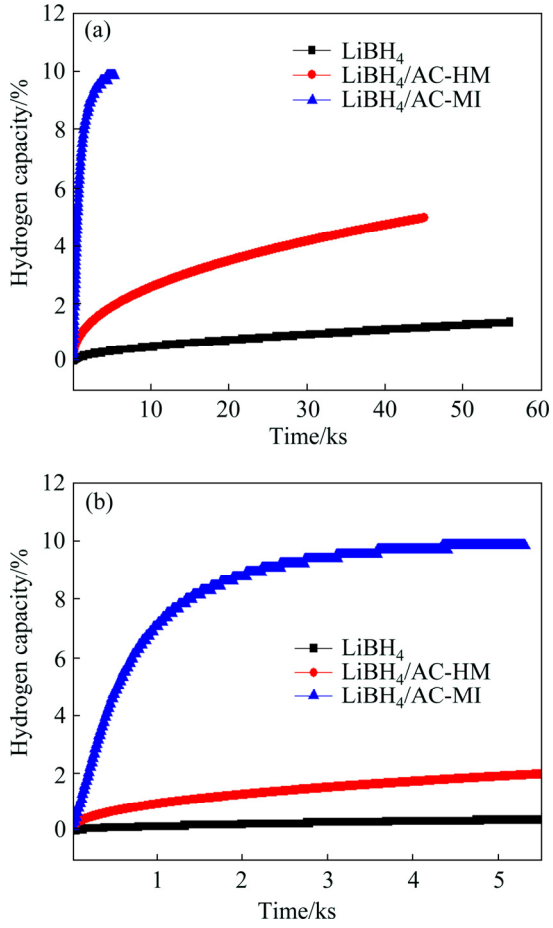

Fig. 6 Isothermal dehydriding curves of $LiBH_4$/AC-MI, $LiBH_4$/AC-HM and pristine $LiBH_4$ at 350 °C

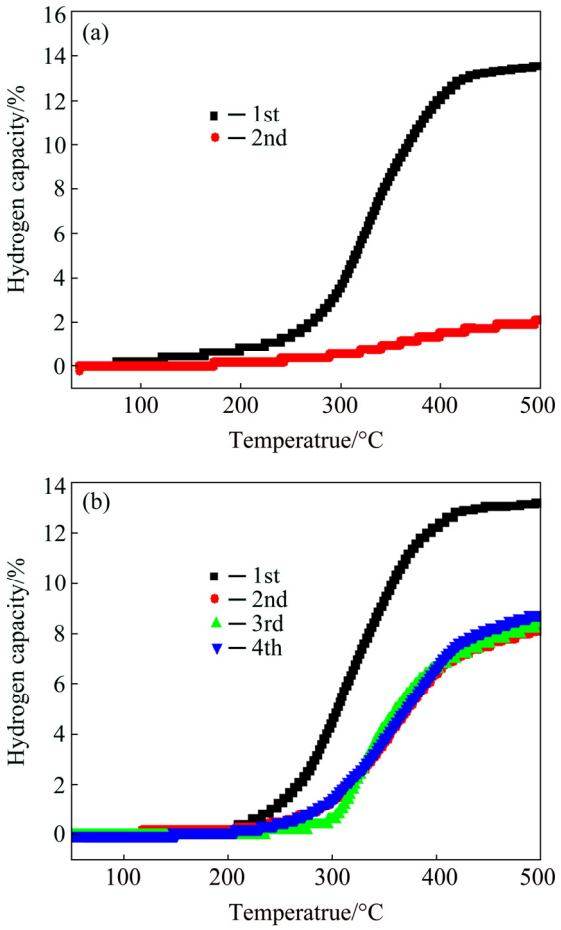

Fig. 7 Cyclic dehydrogenation curves of $LiBH_4$/AC-HM (a) and $LiBH_4$/AC-MI (b)

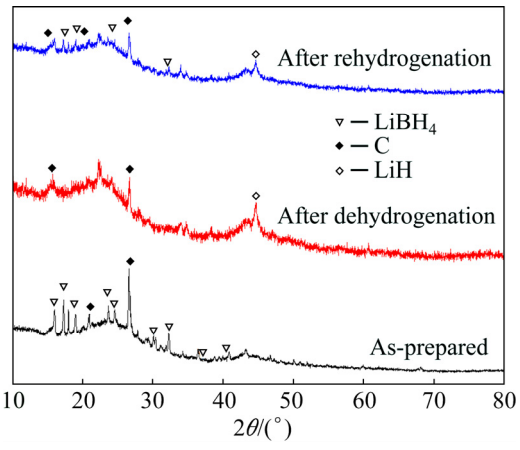

Fig. 8 XRD patterns of as-prepared, dehydrogenated and rehydrogenated $LiBH_4$/AC-MI samples

be seen that $LiBH_4$/AC-HM shows a very bad cycling property. Only about 10% of the hydrogen capacity could be achieved during the second cycle. However, $LiBH_4$/AC-MI has a better cyclic property. During the first three dehydrogenation recycles, 65% of the hydrogen capacity is retained. The rehydrogenation property of $LiBH_4$/AC-MI is much better than that of $LiBH_4$/AC-HM and pure $LiBH_4$. We believe that the reason for the fine cycling property is the nano-confinement effects. As $LiBH_4$ enters into the pore of AC scaffolds, the particle size of $LiBH_4$ becomes much smaller. Thus, LiH and B formed after dehydrogenation also have a much smaller particle size. The carbon scaffolds also serve as a barrier to prevent the formed LiH and B particles from agglomeration. In this case the LiH and small B particles could react with each other easily during the rehydrogenation, which leads to a better rehydrogenate property. Figure 8 shows the XRD patterns of dehydrogenated and rehydrogenated $LiBH_4$/AC-MI. It is clear that $LiBH_4$ is restored after rehydrogenation; however, some diffraction peaks for lithium borohydride still remain, which is caused by the incomplete rehydrogenation.

4 Conclusions

1) Melt infiltration method is an effective way to confine $LiBH_4$ into activated charcoal. The confined $LiBH_4$ can reduce the dehydrogenation temperature. $LiBH_4$/AC-MI starts to decompose at around 190 °C and

finishes the decomposition process at around 400 °C with dehydrogenation capacity of 13.6%.

2) Apparent activation energy of $LiBH_4$/AC-MI is estimated to be 121.1 kJ/mol, which is considerably lower than that of pure $LiBH_4$ (156 kJ/mol). The reduction in the apparent activation energy causes the improvement of dehydrogenation kinetic. $LiBH_4$/AC-MI can release about 9% of hydrogen within 33 min.

3) $LiBH_4$/AC-MI shows good cycling properties, it exhibits a reversibility of up to 65% of its theoretical hydrogen capacity under rehydrogenation condition of 350 °C and 6 MPa H_2.

References

[1] SCHLAPBACH L, ZUTTEL A. Hydrogen-storage materials for mobile applications [J]. Nature, 2001, 414(6861): 353−358.

[2] XIE L S, LI J S, ZHANG T B, KOU H C. Role of milling time and Ni content on dehydrogenation behavior of MgH_2/Ni composite [J]. Transactions of Nonferrous Metals Society of China, 2017, 27(3): 569−577.

[3] SCHUTH F, BOGDANOVIC B, FELDERHOFF M. Light metal hydrides and complex hydrides for hydrogen storage [J]. Chemical Communications, 2004, 20: 2249−2258.

[4] HAN L Y, XIAO X Z, FAN X L, LI Y, LI S Q, GE H W, WANG Q D, CHEN L X. Enhanced dehydrogenation performances and mechanism of $LiBH_4$/$Mg_{17}Al_{12}$-hydride composite [J]. Transactions of Nonferrous Metals Society of China, 2014, 24(1): 152−157.

[5] CHEN C Y, CHEN H L, MA Y Q, LIU J. Hydrogen desorption kinetics mechanism of Mg−Ni hydride under isothermal and non-isothermal conditions [J]. Transactions of Nonferrous Metals Society of China, 2016, 26(1): 160−166.

[6] BOGDANOVIĆ B, SCHWICKARDI M. Ti-doped alkali metal aluminium hydrides as potential novel reversible hydrogen storage materials [J]. Journal of Alloys and Compounds, 1997, 253−254: 1−9.

[7] ZÜTTEL A, WENGER P, RENTSCH S, SUDAN P, MAURON P, EMMENEGGER C. $LiBH_4$ a new hydrogen storage material [J]. Journal of Power Sources, 2003, 118(1−2): 1−7.

[8] UMEGAKI T, YAN J M, ZHANG X B, SHIOYAMA H, KURIYAMA N, XU Q. Boron- and nitrogen-based chemical hydrogen storage materials [J]. International Journal of Hydrogen Energy, 2009, 34(5): 2303−2311.

[9] MAURON P, BUCHTER F, FRIEDRICHS O, REMHOF A, BIELMANN M, ZWICKY C N, ZUTTEL A. Stability and reversibility of $LiBH_4$ [J]. The Journal of Physical Chemistry B, 2008, 112(3): 906−910.

[10] ORIMO S, NAKAMORI Y, KITAHARA G, MIWA K, OHBA N, TOWATA S, Z TTEL A. Dehydriding and rehydriding reactions of $LiBH_4$ [J]. Journal of Alloys and Compounds, 2005, 404−406: 427−430.

[11] VAJEESTON P, RAVINDRAN P, KJEKSHUS A, FJELLV G H. Structural stability and electronic structure for Li_3AlH_6 [J]. Physical Review B, 2004, 69(2): 020104.

[12] PRICE T E C, GRANT D M, LEGRAND V, WALKER G S. Enhanced kinetics for the LiBH4:MgH_2 multi-component hydrogen storage system—The effects of stoichiometry and decomposition environment on cycling behaviour [J]. International Journal of Hydrogen Energy, 2010, 35(9): 4154−4161.

[13] VAJO J J, SKEITH S L, MERTENS F. Reversible storage of hydrogen in destabilized $LiBH_4$ [J]. The Journal of Physical Chemistry B, 2005, 109(9): 3719−3722.

[14] ALAPATI S V, KARL JOHNSON J, SHOLL D S. Using first principles calculations to identify new destabilized metal hydride reactions for reversible hydrogen storage [J]. Physical Chemistry Chemical Physics, 2007, 9(12): 1438−1452.

[15] LI H W, KIKUCHI K, NAKAMORI Y, OHBA N, MIWA K, TOWATA S, ORIMO S. Dehydriding and rehydriding processes of well-crystallized $Mg(BH_4)_2$ accompanying with formation of intermediate compounds [J]. Acta Materialia, 2008, 56(6): 1342−1347.

[16] ALAPATI S V, JOHNSON J K, SHOLL D S. Large-scale screening of metal hydride mixtures for high-capacity hydrogen storage from first-principles calculations [J]. The Journal of Physical Chemistry C, 2008, 112(14): 5258−5262.

[17] SUN T, LIU J, JIA Y, WANG H, SUN D, ZHU M, YAO X. Confined $LiBH_4$: Enabling fast hydrogen release at ~100 °C [J]. International Journal of Hydrogen Energy, 2012, 37(24): 18920−18926.

[18] NIELSEN T K, JAVADIAN P, POLANSKI M, BESENBACHER F, BYSTRZYCKI J, JENSEN T R. Nanoconfined $NaAlH_4$: Determination of distinct prolific effects from pore size, crystallite size, and surface interactions [J]. The Journal of Physical Chemistry C, 2012, 116(39): 21046−21051.

[19] SHANE D T, COREY R L, MCINTOSH C, RAYHEL L H, BOWMAN R C, VAJO J J, GROSS A F, CONRADI M S. $LiBH_4$ in carbon aerogel nanoscaffolds: An NMR study of atomic motions [J]. The Journal of Physical Chemistry C, 2010, 114(9): 4008−4014.

[20] NGENE P, ADELHELM P, BEALE A M, de JONG K P, de JONGH P E. $LiBH_4$/SBA-15 nanocomposites prepared by melt infiltration under hydrogen pressure: Synthesis and hydrogen sorption properties [J]. The Journal of Physical Chemistry C, 2010, 114(13): 6163−6168.

[21] YU X B, GRANT D M, WALKER G S. Dehydrogenation of $LiBH_4$ destabilized with various oxides [J]. The Journal of Physical Chemistry C, 2009, 113(41): 17945−17949.

[22] LI H W, KIKUCHI K, NAKAMORI Y, MIWA K, TOWATA S, ORIMO S. Effects of ball milling and additives on dehydriding behaviors of well-crystallized $Mg(BH_4)_2$ [J]. Scripta Materialia, 2007, 57(8): 679−682.

[23] GENNARI F C. Destabilization of $LiBH_4$ by MH_2 (M = Ce, La) for hydrogen storage: Nanostructural effects on the hydrogen sorption kinetics [J]. International Journal of Hydrogen Energy, 2011, 36(23): 15231−15238.

[24] ZHENG S Y, LI Y T, FANG F, ZHOU G Y, YU X B, CHEN G R, SUN D L, OUYANG L Z, ZHU M. Improved dehydrogenation of TiF_3-doped $NaAlH_4$ using ordered mesoporous SiO_2 as a codopant [J]. Journal of Materials Research, 2011, 25(10): 2047−2053.

[25] FANG Z Z, KANG X D, YANG Z X, WALKER G S, WANG P. Combined effects of functional cation and anion on the reversible dehydrogenation of $LiBH_4$ [J]. The Journal of Physical Chemistry C, 2011, 115(23): 11839−11845.

[26] BRINKS H W, FOSSDAL A, HAUBACK B C. Adjustment of the stability of complex hydrides by anion substitution [J]. The Journal of Physical Chemistry C, 2008, 112(14): 5658−5661.

[27] van SETTEN M J, de WIJS G A, BROCKS G. Ab initio study of the effects of transition metal doping of Mg_2NiH_4 [J]. Physical Review B, 2007, 76(7): 8.

[28] FANG Z Z, WANG P, RUFFORD T E, KANG X D, LU G Q, CHENG H M. Kinetic- and thermodynamic-based improvements of lithium borohydride incorporated into activated carbon [J]. Acta Materialia, 2008, 56(20): 6257−6263.

[29] WARD P A, TEPROVICH J A, PETERS B, WHEELER J, COMPTON R N, ZIDAN R. Reversible hydrogen storage in a $LiBH_4$−C60 nanocomposite [J]. The Journal of Physical Chemistry C, 2013, 117(44): 22569−22575.

[30] GROSS A F, VAJO J J, VAN ATTA S L, OLSON G L. Enhanced hydrogen storage kinetics of $LiBH_4$ in nanoporous carbon scaffolds [J]. The Journal of Physical Chemistry C, 2008, 112(14): 5651−5657.
[31] GUTOWSKA A, LI L, SHIN Y, WANG C M, LI X S, LINEHAN J C, SMITH R S, KAY B D, SCHMID B, SHAW W, GUTOWSKI M, AUTREY T. Nanoscaffold mediates hydrogen release and the reactivity of ammonia borane [J]. Angewandte Chemie International Edition, 2005, 44(23): 3578−3582.
[32] de JONGH P E, ALLENDORF M, VAJO J J, ZLOTEA C. Nanoconfined light metal hydrides for reversible hydrogen storage [J]. MRS Bulletin, 2013, 38(6): 488−494.
[33] NIELSEN T K, B SENBERG U, GOSALAWIT R, DORNHEIM M, CERENIUS Y, BESENBACHER F, JENSEN T R. A reversible nanoconfined chemical reaction [J]. ACS Nano, 2010, 4(7): 3903−3908.
[34] GOSALAWIT-UTKE R, NIELSEN T K, SALDAN I, LAIPPLE D, CERENIUS Y, JENSEN T R, KLASSEN T, DORNHEIM M. Nanoconfined $2LiBH_4$−MgH_2 prepared by direct melt infiltration into nanoporous materials [J]. The Journal of Physical Chemistry C, 2011, 115(21): 10903−10910.

活性炭限域提高硼氢化锂放氢动力学和可逆储氢性能

周 和[1]，刘海镇[2]，高世超[1]，王新华[1]

1. 浙江大学 材料科学与工程学院 硅材料国家重点实验室，杭州 310027；
2. 国家电网全球能源互联网研究院 先进输电技术国家重点实验室，北京 102209

摘 要：通过熔融浸渗法将 $LiBH_4$ 限域于多孔活性炭中，并研究浸渗限域对 $LiBH_4$ 储氢性能的影响。氮气吸附结果表明，熔融浸渗方法能够有效将 $LiBH_4$ 限域于活性炭中。该方法既能够保持活性炭骨架结构完整，又能确保限域的效果。放氢结果表明，活性炭限域 $LiBH_4$ 在 190 °C 开始放氢，该起始放氢温度比纯 $LiBH_4$ 低 160 °C，并且在 400 °C 时放氢容量达到 13.6%。放氢后样品在 6 MPa 氢压和 350 °C 下再吸氢，可逆储氢容量达到 6%，而在相同条件下，纯 $LiBH_4$ 几乎没有可逆储氢容量。质谱分析结果表明，放氢过程中没有乙硼烷和其他杂质气体放出。活性炭限域的 $LiBH_4$ 放氢表观活化能由 156.0 kJ/mol 降低到 121.1 kJ/mol，使 $LiBH_4$ 放氢动力学性能得到显著改善。

关键词：储氢材料；储氢性能；硼氢化锂；活性炭；熔融浸渗

(Edited by Xiang-qun LI)